JOURNAL OF THE MECHANICAL BEHAVIOR OF BIOMEDICAL MATERIALS 29 (2014) 317–327

Available online at www.sciencedirect.com

ScienceDirect

www.elsevier.com/locate/jmbbm

Research Paper

Enhancing glass ionomer cement features by using the HA/YSZ nanocomposite: A feed forward neural network modelling

Ghadir Rajabzadeh[a,*], *Sahar Salehi*[b], *Ali Nemati*[c], *Razeih Tavakoli*[d], *Mehran Solati Hashjin*[e,f]

[a]*Nanotechnology Department, Research Institute of Food Science and Technology, Mashhad, Iran*
[b]*Department of Material Engineering, Science and Research Branch, Islamic Azad University, Tehran, Iran*
[c]*Department of Materials Science & Engineering, Sharif University of Technology, Tehran, Iran*
[d]*Department of Computer, Mashhad Branch, Islamic Azad University, Mashhad, Iran*
[e]*Department of Biomedical Engineering, Faculty of Engineering, University of Malaya, Kuala Lumpur 50603, Malaysia*
[f]*Nanobiomaterials Laboratory (NBML), Biomaterials Center of Excellence, Amirkabir University of Technology, Tehran 15914, Iran*

ARTICLE INFO

Article history:
Received 2 June 2013
Accepted 26 July 2013
Available online 28 August 2013

Keywords:
Dental cements
Microhardness
Diametral tensile and compressive strength
Fluoride release
HA/YSZ nanocomposite
GIC
Feed forward neural network

ABSTRACT

Despite brilliant properties of glass ionomer cement (GIC), its weak mechanical property poses an obstacle for its use in medical applications. The present research aims to formulate hydroxyapatite/yttria-stabilized zirconia (HA/YSZ) in the composition of GIC to enhance mechanical properties and to improve fluoride release of GIC. HA/YSZ was synthesized via a sol–gel method and characterized by applying X-ray diffraction (XRD), Fourier transform infrared spectroscopy (FT-IR), X-ray photo-emission spectroscopy (XPS) and simultaneous thermal analysis (STA) along with transmission electron microscopy (TEM) methods. The synthesized nanocomposite was mixed with GIC at a fixed composition of 5 wt%. The effect of different weight percentages of YSZ:HA on GIC was investigated by measuring the compressive strength, diametral tensile strength, microhardness and fluoride release. The results showed that, after 1 and 7 days of setting, the 20 wt% nanohydroxyapatite/80 wt% stabilized zirconia cement exhibited higher compressive strength (1857–245 MPa), higher diametral tensile strength (11–14 MPa) and greater microhardness (104–106 MPa) as compared with the pure GIC (65–88 MPa in compressive strength, 5–9.5 MPa in diametral tensile strength and 70–89 MPa in microhardness). The reinforced cement, also, exhibited higher fluoride release compared with pure GIC.

The artificial neural network (ANN) was trained for modeling the system. Results obtained by ANN have proved to be completely in accordance with expectations.

*Corresponding author. Tel.: +98 5115003209; fax: +98 5115003150.
E-mail address: gh.rajabzadeh@rifst.ac.ir (G. Rajabzadeh).

1751-6161/$ - see front matter © 2013 Elsevier Ltd. All rights reserved.
http://dx.doi.org/10.1016/j.jmbbm.2013.07.025

1. Introduction

Glass ionomer cement was synthesized for the first time by Wilson in 1971 (Wilson and Kent, 1971). It contained glass powder and carboxylic acids as an ionomer (Goenka et al., 2012). The unique properties of GIC such as adhesion to moist teeth, anti-carcinogenic character, lack of exothermic polymerization, excellent adhesion to bone, close thermal expansion to tooth, satisfactory biocompatibility, made it as an important material in dental applications (Goenka et al., 2012). Moreover, GIC has been used as a restorative material in orthopedic surgery (Gu et al., 2005a, 2005b). Besides these beneficial characteristics, the cement suffers from weak mechanical properties like brittleness, low strength and toughness (Goenka et al., 2012; Gu et al., 2005a, 2005b). Using reinforcement phases such as zirconia, hydroxyapatite, N-vinyl pyrrolidone, fluoroapatite, and HA/ZrO_2, is a well-known method to enhance GIC mechanical properties (Goenka et al., 2012; Gu et al., 2005a, 2005b; Moshaverinia et al., 2008). The similarity between HA and natural bone and teeth in both chemical and crystal structure makes it an exclusive choice to improve GIC properties (Lucas et al., 2003). On the other hand, high strength, fracture toughness and biocompatibility of zirconia make it as a superior option for the reinforcement of biomaterial cements used in hip replacement and dental filler (Cales et al., 1994; Uo et al., 2003; Gu et al., 2005a, 2005b). The tooth-color of YSZ (from white to yellow) is its unique property for dental application (Gu et al., 2005a, 2005b). MgO, CaO, Y_2O_3 and CeO were used to stabilize zirconium in a proper phase (Lee et al., 2002). The superior biocompatibility of HA and the advanced mechanical properties of YSZ have made the HA/YSZ nanocomposite an appropriate option for the development of GIC based materials (Gu et al., 2005a, 2005b).

Different methods have been applied for the synthesis of HA-based ceramics, such as co-precipitation (Sung et al., 2007), solid-state reaction (Chiu et al., 2007), and sol–gel methods (Feng et al., 2005). The material produced by the sol–gel process is more chemically and physically homogenized than that produced by a conventional method (Salehi and Fathi, 2010). The sol–gel method does not require a high pH value or intense thermal treatment, and the obtained powder has a higher surface area.

ANN technique, a sub-field of artificial intelligence, has been used to solve a wide variety of problems in engineering fields since 1994. ANN can automatically develop the complex and nonlinear relationships between input and output signals of trained data. Recently, the study of the mechanical property of materials by the use of the neural network has been presented in several articles (Hwang et al., 2010). The results have successfully shown the possibility and the feasibility of the neural network in the field of material science.

In this study, the synthesis and characterization of the HA/YSZ nanocomposite is investigated. A feed forward neural network along with experimental study is carried out to predict the influence of the HA/YSZ ratio on mechanical properties and fluoride release of the GIC. The results obtained from ANN are in line with the experimental results and ANN effectively predicted the mechanical properties and fluoride release of the system.

2. Materials and methods

2.1. Material

Zirconium (IV) propoxide and yttrium (III) nitrate hexahydrate were obtained from Sigma-Aldrich Chemical Co. (Milwaukee, WI, USA). Calcium nitrate tetrahydrate (CNT), potassium dihydrogen phosphate (KDP) and acetic acid were purchased from Merck Chemical Co. (Germany). All chemicals used in this study were of AR analytical grade.

Fuji IX GP A3 shade (GC Corporation Japan) was applied as the GIC base.

2.2. Synthesis of the HA–ZrO_2–Y_2O_3 nanocomposite

The HA sol was prepared through the method reported by Sanosh et al. (2009). Briefly, CNT and KDP were used as calcium and phosphorous source. The ratio of calcium to phosphor in solution was kept at 1.67, as it was in the HA content; KDP (0.6 M) was dissolved in deionized water. Then, the aqueous solution of the CNT was added drop by drop to the KDP solution and the obtained sol was vigorously stirred for 24 h in a plastic-wrapped glass container.

The preparation of the stabilized zirconia was according to the previously reported procedure by Salehi and Fathi (2010). In brief, zirconium (IV) propoxide (70% solution) was diluted in 1-propanol. Then, acetic acid was added drop by drop to the solution to achieve hemogenization by a complex formation. Yttrium (III) nitrate hexahydrate (3 mol%) and deionized water were added to the mixture and the obtained sol was vigorously stirred for 24 h. The molar ratio of H_2O to Zr, 1-propanol to Zr and acetic acid to Zr were 10–1, 50–1, and 5–1, respectively. The zirconium sol was added drop by drop to the HA sol, and the mixture was vigorously stirred for 24 h. Finally, the obtained sol was aged for 4 h at room temperature. The gel was dried at 80 °C and calcinated at 750 °C for 1 h.

The different weight percentages of HA to YSZ were prepared according to the mixture design method. The coordinates of the five design points were generated and arranged randomly by Minitab 14 software. The respective nanocomposite formulations are presented in Table 1.

Table 1 – The chemical composition of nanocomposite

Proportion of the components			
Sample code	HA (wt%)	ZrO_2 (wt%)	Y_2O_3 (wt%)
NBC+301	70	28.44	1.56
NBC+302	20	75.83	4.17
NBC+303	45	52.13	2.87
NBC+304	57.5	40.28	2.22
NBC+305	32.5	63.9	3.52

2.3. Preparation of the HA/YSZ–GIC nanocomposite

In this study, Fuji IX was used as the test control and contained fluoro-alumino-silicate glass, polyacrylic acid, polybasic carboxylic acid and water. Five weight percentages of the fluoro-alumino-silicate powder in Fuji IX were replaced by different samples of the HA/YSZ nanocomposite to achieve an optimum weight percentage of HA: YSZ in GIC formulation.

The glass powder and HA/YSZ were mixed manually before its addition to the polyacid liquid. The recommended powder rather to liquid was according to the British Standards 6039-1981 for dental GICs (Dental standard BS 6039:1981). Next, the mixture was directly inserted into molds. Samples were immersed in deionized water for 1 and 7 day periods at 37 °C and intended for mechanical and fluoride release testing.

2.4. Characterization

2.4.1. HA/YSZ characterization

The thermal behavior of the dried gel was examined with STA Bahar 503 during heating from 20 to 1200 °C (10 °C/min). Phase characterization of nanopowders was carried out by using the XRD (XMD-300 powder diffractometer (Unisantis) with Co Kα irradiation (Mn filter)). The chemical conjunction of nanocomposites was analyzed with Nicolet FT-IR spectrophotometer. The spectra were recorded from 4000 to 500 cm^{-1}. A further investigation of the composition and chemical state of the prepared nanocomposite was performed by applying the XPS analysis. The XPS was carried out on a VG Microtech, twin-anode XR3E2 X-ray source using Al Kα=1486.6 eV and the air pressure in the vacuum chamber was below 10^{-8} Pa. The TEM (Zeiss Leo 912 AB) was utilized to evaluate the morphology and particle size of the synthesized nanocomposite. The distribution of nanoparticles in the GIC matrix was done on a Zeiss Leo 440i SEM.

2.4.2. Mechanical test

2.4.2.1. Microhardness testing. Molds for microhardness test had an internal dimension of 4 mm in height and 8 mm in diameter. The Vickers microhardness measurement was performed with a microhardness tester (Matsuzawa, MHT2, and Japan). A 50 gf load was applied through the indenter with a dwell time of 30 s. Five experiments were conducted for each sample.

2.4.2.2. Compressive strength testing. The compressive strength testing was performed according to the dental GICs' British Standard 6039-1981 by a Santam testing machine (Santam, STM-50, Iran) (Dental standard BS 6039:1981). Five samples ($6 \times 12\ mm^2$) were tested after they have been soaked in de-ionized water for 1 and 7 day periods. The compressive strength, C (MPa), was calculated by using the following equation:

$$C = 4P/\pi D^2 \quad (1)$$

in which P is the maximum applied load (N) and D is the sample diameter (mm).

2.4.2.3. Diametral tensile strength testing. The diametral tensile strength testing was performed based on dental GICs' British Standards 6039-1981 (Dental standard BS 6039:1981). Five samples ($8 \times 4\ mm^2$) were tested with a Santam testing machine (Santam, STM-50, Iran) after soaking in deionized water for 1 day and 7 day periods. The diametral tensile strength, T (MPa), was calculated by using the following equation:

$$T = 2P/\pi DL \quad (2)$$

in which P is the maximum applied load (N), D is the sample diameter (mm) and L is the height of the sample (mm).

2.4.2.4. Fluoride release experiment. Samples ($8 \times 4\ mm^2$) were immersed in the 25 mL deionized water and stored in an incubator at 37 °C for various amounts of time. The fluoride ion concentration in the water was determined by Hach DR5000 at various immersion periods. Samples were taken out of the deionized water, dried with filter paper, and immediately immersed in 25 mL of fresh water.

2.5. Artificial neural network

The intellectual heuristic methods are based on neural networks, Fuzzy Logic Evolutionary Algorithms and hybrid intelligent systems. In contrast to the classical statistical methods, the utmost merit of these methods is the assistance they provide for designers to access a complex nonlinear system with which to model the actual dynamic phenomenon is modeled. The other merit of heuristic methods is that, unlike the classical methods, a pattern is not required and no distribution of observation data is ascertained.

An ANN is a computational model that is inspired by the structure and/or functional aspects of biological neural networks. A neural network consists of an interconnected group of artificial neurons and processes information by using a connectionist approach to computation. In most cases, an ANN is an adaptive system that changes its structure based on external or internal information flowing through the network during the learning phase. The modern neural networks are usually employed to model complex relationships between inputs and outputs in order to identify patterns in data.

2.5.1. Feed forward neural network

Feed forward multilayers are mathematical structures that can be trained by pairs of input and output data used as learning data values. The learned knowledge is memorized in terms of the state of these weights as well as the biases. These systems are composed of a network of processing units called neurons, which perform the weighted sum of inputs and use the resulting sum as the argument of a nonlinear activation function. The activation functions are sharp threshold functions, which have evolved to piecewise linear saturation functions to differentiable saturation functions (or sigmoid). The number of neurons at the input and the output layer is fixed to be equal to that of input and output variables. The input layer consists of all the input factors, such as the HA, ZrO_2 and Y_2O_3, immersion time and cement

weight percentages, and the output layer includes fluoride release, diametral tensile strength, compressive strength and microhardness. The hidden layers can be used in more than one layer, in which the number of neurons is flexible. Adjusting the structure of a network, namely the number of hidden layers and neurons, is one of the main ways to improve its performance. The decision as to the number of neurons used in the hidden layer usually depends on the arithmetical mean of the number of inputs and outputs (Ozerdem and Kolukisa 2009). The scheme of the feed forward neural network in regard to the general architecture used in this research is illustrated in Fig. 1.

Two hidden layers are used in this application. Information from the input layer is processed in the course of two hidden layers; the following output vector is computed in the final (output) layer. The data inputs are modulated by the transfer function with weights and biases in the neurons of every layer to compute the outputs, as described through the following equation:

$$a = f(\sum_i IW^{(n)}{}_{ji} a_i^{(n-1)} + b_j^{(n)}) \quad (3)$$

where $a_j^{(n)}$ is the output of node j in the nth layer, $IW^{(n)}{}_{ji}$ is the weight from node i in the $(n-1)$th layer to node j in the nth layer, and $b_j^{(n)}$ is the bias of node j in the nth layer. The current research's non-linear transfer function $f(x)$ is a tan-sigmoid function (Eq. 4):

$$f(x) = (1-e^{-2a})/1+e^{-2a} \quad (4)$$

A schematic description of the layers is given in Fig. 2.

In developing a feed forward model, the available data are divided into two sets: one for the training of the network and the remaining set to verify the generalization capability of the network (Ozerdem and Kolukisa, 2009).

The input and output data to design the feed forward in this research are provided in Tables 2–4.

A back-propagation algorithm called BP is an interactively gradient descent method to minimize the mean squared error, E, between the predicted and target outputs. It is one of the most widely used training algorithms for multilayer

Table 2 – The input quantities used in feed forward

HA (wt%)	ZrO_2 (wt%)	Y_2O_3 (wt%)	Time (days)	Cement (wt%)
70	28.44	1.56	1	95
20	75.83	4.17	1	95
45	52.13	2.87	1	95
57.5	40.28	2.22	1	95
32.5	63.98	3.52	1	95
0	0	0	1	100
70	28.44	1.56	7	95
20	75.83	4.17	7	95
45	52.13	2.87	7	95
57.5	40.28	2.22	7	95
32.5	63.98	3.52	7	95
0	0	0	7	100

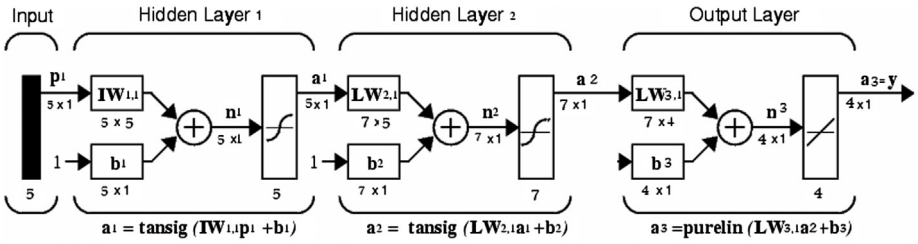

Fig. 1 – The general architecture of an applied feed forward network.

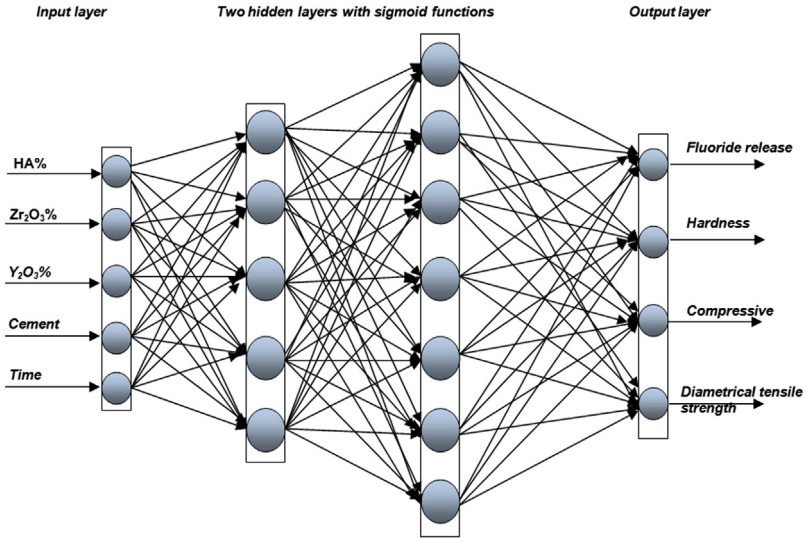

Fig. 2 – The structure of the four layered feed forward neural network proposed in the present study.

Table 3 – The output quantities used in feed forward after 1 day

Trained sample	Microhardness (MHV)	Compressive strength (MPa)	Diametral tensile strength (MPa)	Fluoride release (ppm)
GIC+NBC301	75	84	6.4	14.75
GIC+NBC302	104	185	11	8.5
GIC+NBC303	88	151	10.5	7.87
GIC+NBC304	75	141	7.4	12.87
GIC+NBC305	99	204	12	8.5
Pure GIC	70	65	5	3.6

Table 4 – The output quantities used in feed forward after 7 days

Trained sample	Microhardness (MHV)	Compressive strength (MPa)	Diametral tensile strength (MPa)	Fluoride release (ppm)
GIC+NBC301	90	100	10.6	12.5
GIC+NBC302	106	245	14	11.375
GIC+NBC303	95	235	12.5	8.125
GIC+NBC304	92	149	11	11.5
GIC+NBC305	103	260	15	4.9
Pure GIC	89	88	9.5	4.9

Table 5 – The feed forward architecture and training parameters

The number of layers	4
The number of neuron on the layers	Input layer: 5, first hidden layer: 5, second hidden layer: 7, output layer: 4
The initial weights and biases	Randomly between (−1, 1)
Activation function for hidden and output layers	Tan-sigmoid–tan-sigmoid–pure line
Training parameter learning rules	Back-propagation
Adaptive learning-rate for hidden layers	From 0.9 to 0.887583
Number of iteration	100
Momentum constant	0.95
Duration of learning time	1 min 27 s
Acceptable mean-squared error	0.05

networks. The average square error in this method is calculated by the following equation:

$$E = 1/2m\left(\sum_{t=1}^{m}(T(t)-P(t))^2\right) \quad (5)$$

where m shows the number of training data, $T(t)$ refers to target output values, and $P(t)$ is network outputs or predicted data. The feed forward network architecture and training data, which are employed in the feed forward neural network learning stage, are given in Table 5.

3. Result and discussion

3.1. *Characterization of nanocomposite*

The thermal behavior of HA–YSZ is shown in Fig. 3. 40 mg of dried gel was heat treated up to 1200 °C along with alumina as a reference material. The total weight loss for the nanocomposite was about 50% in the range of 25–1200 °C. A weight loss happening between 25 and 100 °C, which was correlated to an endothermic peak, was recognized by the evaporation of the absorbed water (Sanosh et al., 2009). A weight loss occurring between 150 and 200 °C is corresponded to the evaporation of the bonded H_2O and the organic compounds, such as 1-propanol (Sanosh et al., 2009). The second exothermic peak at 550 °C was related to the crystallization of the tetragonal structure of zirconium (Hwang et al., 2010).

The increase in the peak area happened around 1000 °C, which was due to the decomposition of HA to tricalciumphosphate (TCP) (Balamurugan et al., 2007). According to the data obtained, calcination of the HA–YSZ composite was performed at 750 °C. Fig. 4 illustrates the XRD pattern of the nanocomposite calcinated at 750 °C.

The absence of free yttria in XRD diagram proves the formation of a solid solution of Y_2O_3 in ZrO_2 (Salehi and Fathi, 2010). The appearance of t-ZrO_2 at this low temperature is related to the influence of the hydroxyl groups in the HA matrix (Sliva and Lameiras, 2000). According to the XRD pattern, HA is stable at the operating calcination temperature.

The monoclinic ZrO_2, decreases the HA decomposition temperature due to the transfer of CaO to the zirconia matrix and results in the formation of β-TCP and CaO as HA decomposition products (Piconi and Maccauro, 1999). When zirconia is stabilized with Y_2O_3, tetragonal structure of ZrO_2-with no monoclinic phase is formed (Piconi and Maccauro, 1999). The YSZ is less reactive to CaO than the pure ZrO_2.The Y_2O_3 fills the vacancies of the ZrO_2 structure and decreases the diffusion rate of CaO in ZrO_2 lattice, which leads to the building up of $CaZrO_3$ on the ZrO_2 surface, instead of diffusion into the ZrO_2 lattice (Guo et al., 2003).

The structure of the HA–YSZ was investigated with FT-IR spectroscopy (Fig. 5). The absorption occurring at 1042 cm^{-1} specifies the Zr–O–Si bond formation (Zhan and Zeng, 1999). Absorption at 414 cm^{-1} is related to the P–O bond of HA, and absorption bond at 560 cm^{-1} belongs to the O–H bending (Sliva and Lameiras, 2000). The absorption bond observed at 590 cm^{-1} demonstrated the existence of the t-ZrO_2 phase (Monte et al., 2000).

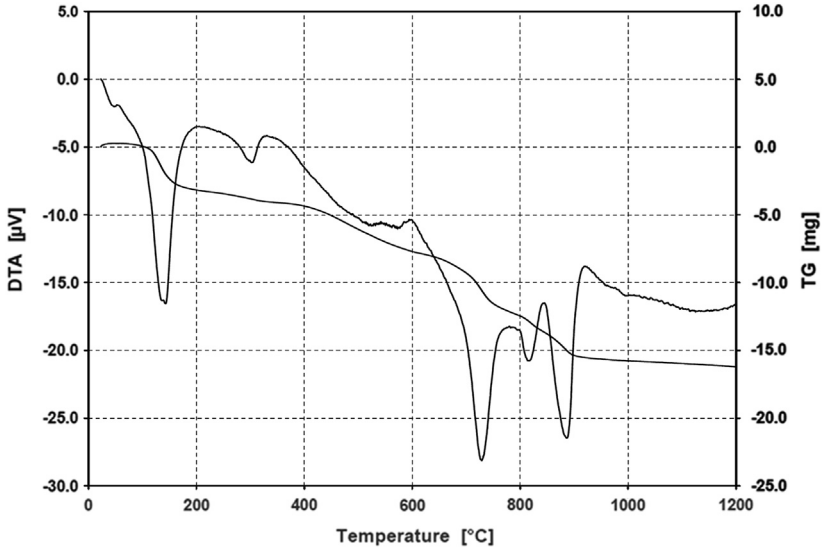

Fig. 3 – The STA curves of the HA/YSZ nanocomposite.

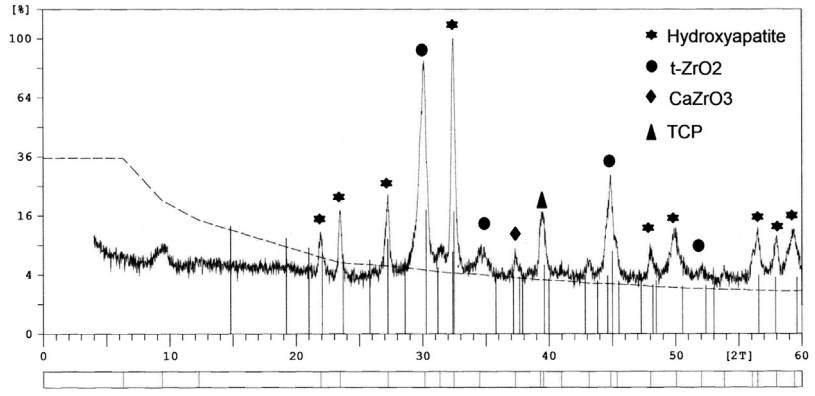

Fig. 4 – The XRD pattern of HA/YSZ calcinated at 750 °C.

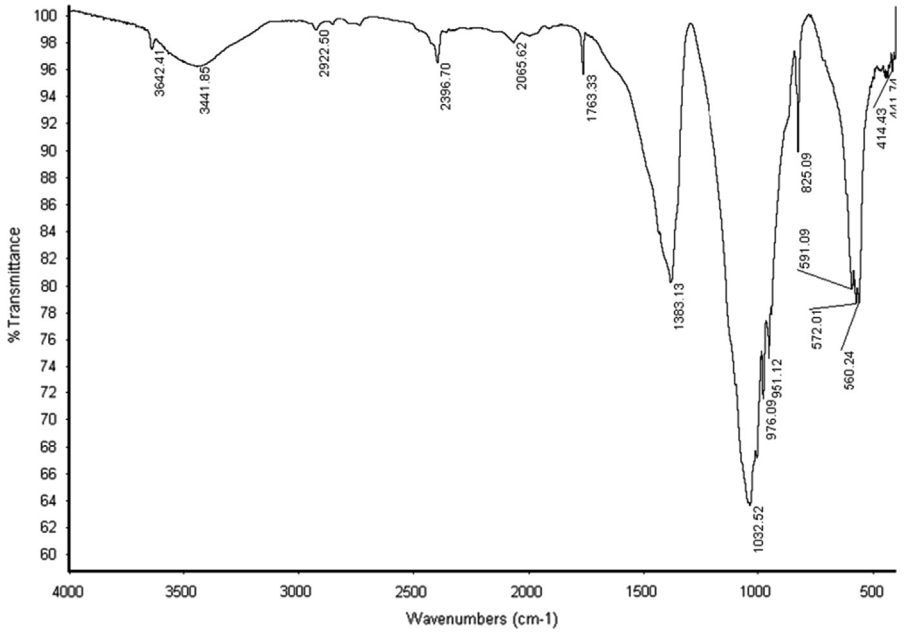

Fig. 5 – The FT-IR spectra of HA/YSZ nanocomposite.

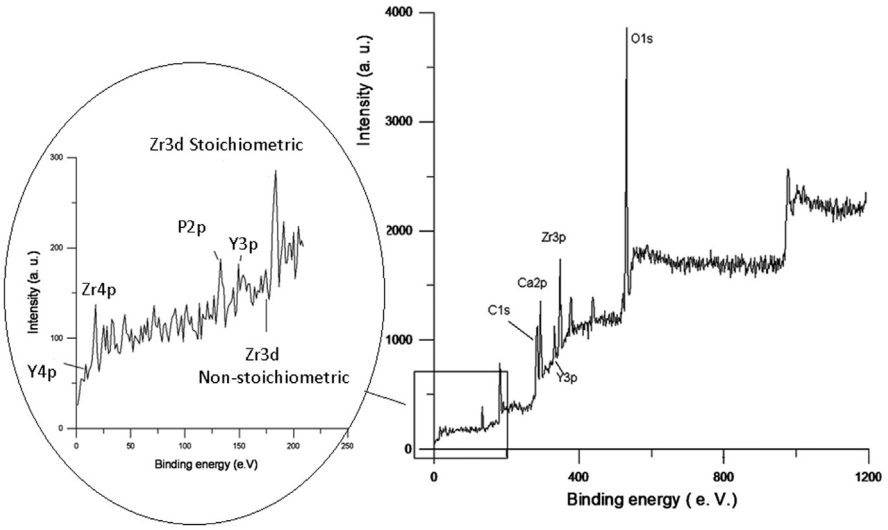

Fig. 6 – The XPS survey of the HA/YSZ nanocomposite.

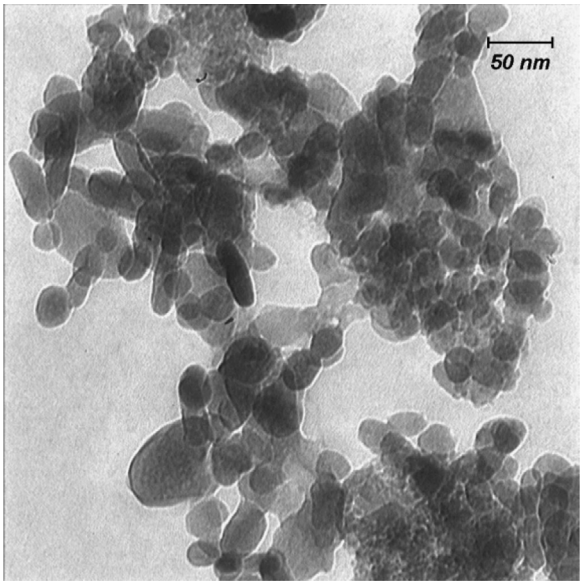

Fig. 7 – The TEM image of the HA/YSZ nanocomposite.

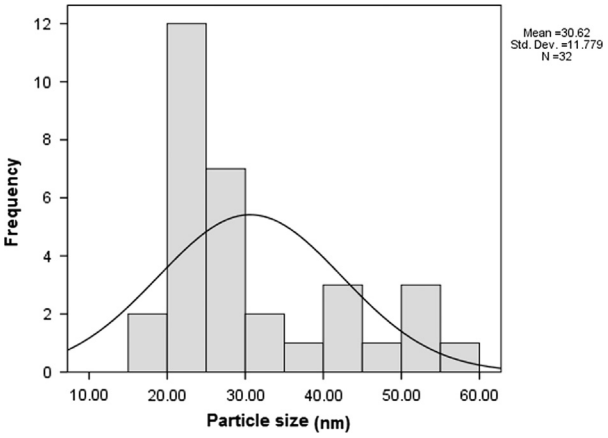

Fig. 8 – The particle size distribution of the HA/YSZ.

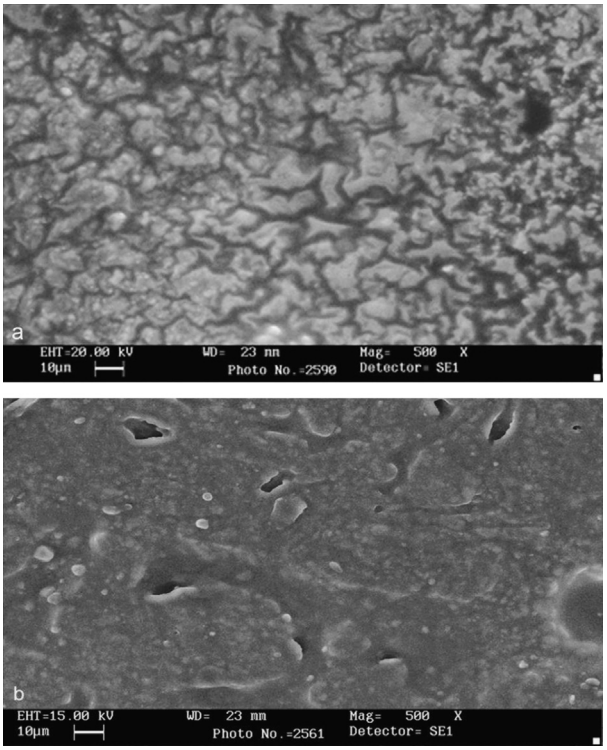

Fig. 9 – The SEM image of GIC (a) and HA/YSZ–GIC (b).

Further investigation of the composition of the prepared nanocomposite was carried out by using XPS analysis.

The corresponding experimental results, which are shown in Fig. 6, were interpreted according to the C (1s) core level binding energy at 285.0 eV. Reported values of the O1s for ZrO_2 and OH groups in the hydroxyapatite were 530 and 531.8 eV, respectively (Samanipour et al., 2011). However, in this research, O1s were observed at 531.5 eV. The appearance of O1s at 531.5 reflected the conjunction of ZrO_2

and HA. The binding energy located at 183.6 eV was associated to the stoichiometric form of ZrO_2 (Samanipour et al., 2011). The core level of P2p and Ca 2p3, which appeared at 133 and 350 respectively, proved the existence of phosphor and calcium in the HA structure (Chandradass et al., 2008). The binding energy for Y4p appeared at 16.16 eV.

The TEM image of the HA/YSZ is illustrated in Fig. 7. It seems that the spherical darker points belong to YSZ and of cubic lighter points to HA particles (Salehi and Fathi, 2010). Fig. 7, also, represents the fine dispersion of YSZ in the HA matrix.

Particle size distribution of the nanocomposite is shown in Fig. 8. Two typical ranges of particle sizes are illustrated in Fig. 8. The first group is within the range of 15–30 nm and the second one in the range of 30–60 nm, with the major distribution around 30 nm.

Fig. 9 shows the cross-sectional view of pure GIC and HA/YSZ–GICs by SEM. According to the SEM image, a fine dispersion of the particles in the matrix and an acceptable bonding between the glass and the hydrogel salt matrix has occurred. In spite of the TEM of the HA/YSZ, the SEM image of the HA/YSZ–GIC showed that HA/YSZ nanoparticle sizes were more than 100 nm. This is due to the formation of HA/YSZ agglomeration in GIC matrix.

3.2. *Fluoride release profile*

The amount of fluoride release of five reinforced cements in the nine storage periods is shown in Fig. 10. HA/YSZ-loaded cements maintained a higher quantity of fluoride release throughout the experimental period than the pure GIC. The majority of samples had the highest elution during the 14th day and a gradual decrease was observed until the 56th day.

The fluoride release originated entirely from the fluoride containing alumino-silicate glass. Calcium released as HA partially dissolved up its on contact with the acid, which might contribute to the matrix formation. It was diffused through this matrix and/or decomplexation of the fluoride in the polysalt matrix, which was responsible for the long-term fluoride release of GIC (Dhondt et al., 2001).

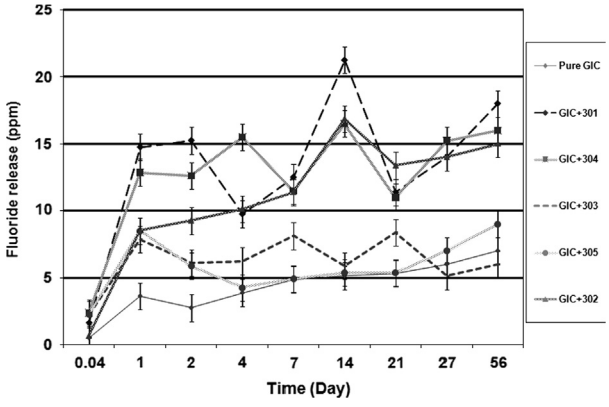

Fig. 10 – The fluoride release profile of HA/YSZ–GIC.

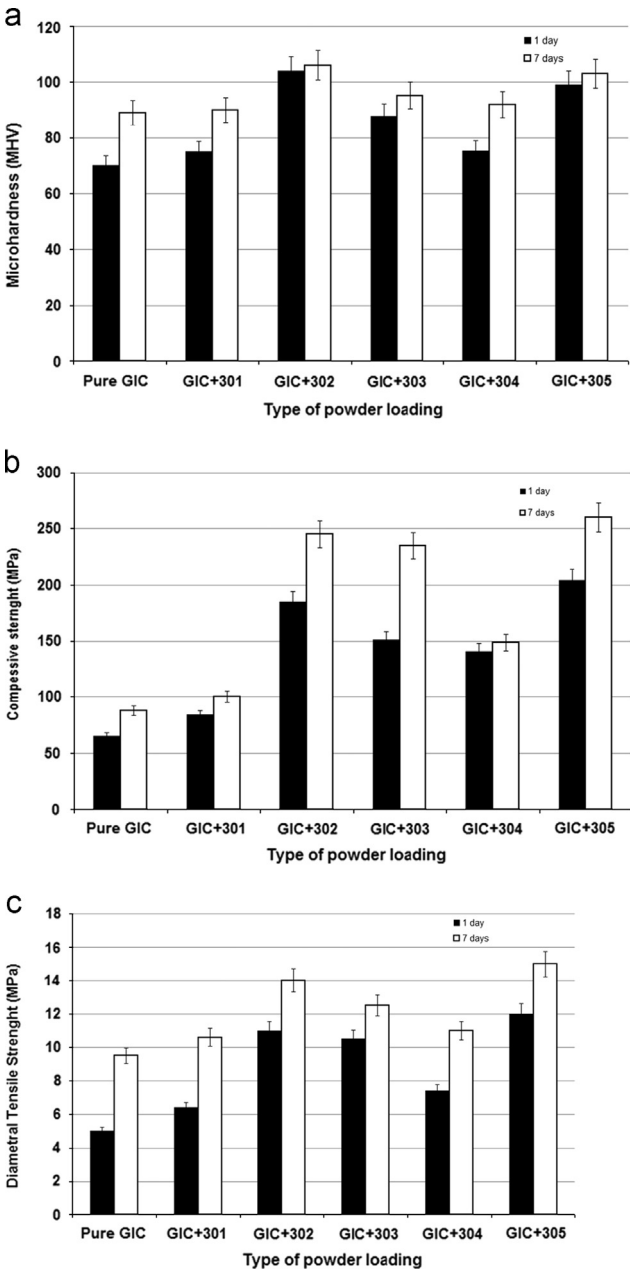

Fig. 11 – The mechanical properties of the HA/YSZ–GIC after 1 and 7 days: microhardness (a), compressive (b), and diametral tensile strength (c).

3.3. *Mechanical properties*

Fig. 11 illustrates the mechanical properties of HA/YSZ–GIC composites and pure GIC which were tested after being saturated in the deionized water for one and seven day periods. Data in Fig. 11 demonstrate the significant difference between the reinforced cement and the pure one. Compared with the pure GIC, the YSZ–GIC composites exhibited considerably higher microhardness, compressive strength, and diametral tensile strength values. The results, also, exhibited a linear correlation between the mechanical properties of HA/YSZ–GIC and ZrO_2 weight percentages in the range of 28–75. That was related to the high strength and hardness of zirconia compared with GIC and HA. Moreover, zirconia did not dissolve in the deionized

Table 6 – The predicted performance of HA/YSZ–GIC parameters after 1 day immersion

HA (wt%)	ZrO_2 (wt%)	Y_2O_3 (wt%)	Fluoride release (ppm)	Microhardness (VHN)	Compressive strength (MPa)	Diametral tensile strength (MPa)
10.32	85	4.6	8.13	98.2	205.88	13
15.6	80	4.4	8.02	99.12	210.89	12.5
18	76.49	4.5	7.95	99.61	212.66	14.37
20	75.83	4.17	8.5	99.68	214	14.37
21	74.65	4.34	7.91	99.85	214.92	14.4
23	72.76	4.23	7.9	99.99	215.62	14.41
25	70.85	4.125	7.89	100	215.96	14.41
27	68.99	4	7.9	100	215.86	14.38
32.5	63.98	3.52	8.12	99.5	214.5	14
35	61.42	3.57	8.31	98.9	207.11	13.87
38	58.9	3.41	8.67	97.43	197	13.39
40	56.7	3.3	9.21	95.96	186.92	12.95
43	53.65	3.135	10.1	93.14	167.1	12.1
45	52.13	2.87	8	92.98	151.82	11.4
50	47.25	2.75	12.17	87.23	122.02	9.87
57.5	40.28	2.22	13.27	80	97.77	8.41
60	37.8	2.2	13.43	84.3	94.06	8.16
70	44.28	1.56	13.58	80	87.67	7.8
78.9	20	1.1	13.23	83.5	88.24	8.02

Table 7 – The predicted performance of HA/YSZ–GIC parameters after 7 day periods immersion

HA (wt%)	ZrO_2 (wt%)	Y_2O_3 (wt%)	Fluoride release (ppm)	Microhardness (VHN)	Compressive strength (MPa)	Diametral tensile strength (MPa)
10.32	85	4.6	7.51	101.27	222.92	15.02
15.6	80	4.4	7.47	10.4	223.62	15.07
18	76.49	4.5	7.46	101.43	223.76	1.08
20	75.83	4.17	7.45	101.46	223.94	15.89
21	74.65	4.34	7.45	101.47	223.91	15.1
23	72.76	4.23	7.45	101.48	223.96	15.09
25	70.85	4.125	7.45	101.48	223.96	15.1
27	68.99	4	7.45	101.48	223.91	15.08
32.5	63.98	3.52	4	101.41	223	15.04
35	61.42	3.57	7.5	101.33	22.82	14.98
38	58.9	3.41	7.57	101.18	221.77	14.89
40	56.7	3.3	7.61	101.02	220.69	14.8
43	53.65	3.135	7.02	100.66	218.18	14.61
45	52.13	2.87	7.85	10.24	215.39	14.44
50	47.25	2.75	12.17	87.22	122.03	9.87
57.5	40.28	2.22	11.37	91.95	158	1.72
60	37.8	2.2	11.12	89.87	141.5	10.9
70	44.28	1.56	12.88	84.81	99.91	8.69
78.9	20	1.1	12.26	83.73	92.04	8.43

water while soaking. After being soaked for 7 days, the mechanical properties of cement were still quite satisfactory in the presence of zirconia. The results were in a good agreement by the findings of Gu et al. (2005a, 2005b). The distribution of small HA/ZrO_2 particles within large particles of GIC powder produced an increasing by packing density within the ionomer matrix and, thus, improved GIC mechanical properties (Noort, 1994).

The mechanical properties of HA/YSZ–GIC were enhanced during the immersion time. This could be attributed to the increase in the degree of cross-linking of the polymer molecules by the formation of aluminum salt bridges (Heffernan et al., 2002).

3.4. *The predicted results for GIC properties by the feed forward neural network*

The aim of the feed forward neural network as a subdivision of ANN is to predict the GIC behavior as a consequence of changes in components concentration. The predicted results for GIC parameters are summarized in Tables 6 and 7.

The comparison of the measured and the predicted data of GIC properties at the validation stage are presented in Figs. 12 and 13. A combination of HA 20 wt% and YSZ 80 wt% exhibited optimum characteristics for mechanical and fluoride release properties. A high correlation between the predicted and examined results reflected a well-trained ANN.

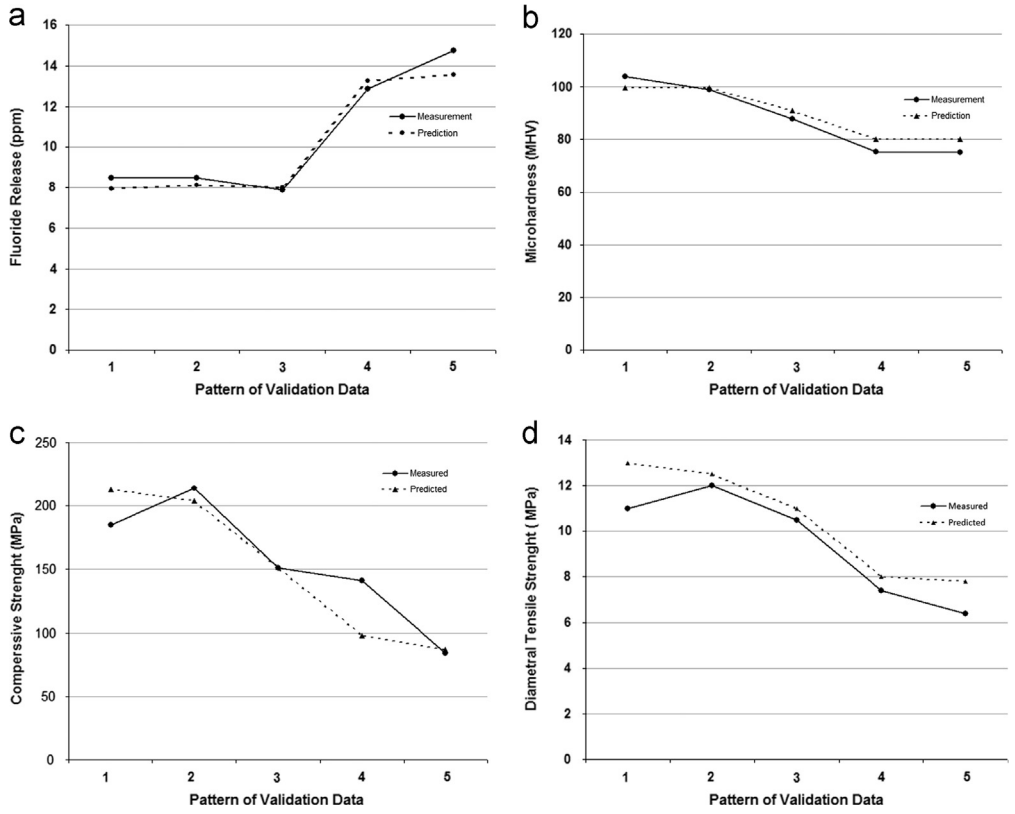

Fig. 12 – The comparison of the measured and the predicted data for the test stage of fluoride release (a), microhardness (b), compressive strength (c) and diametral tensile strength (d) of HA/YSZ–GIC after 1 day immersion.

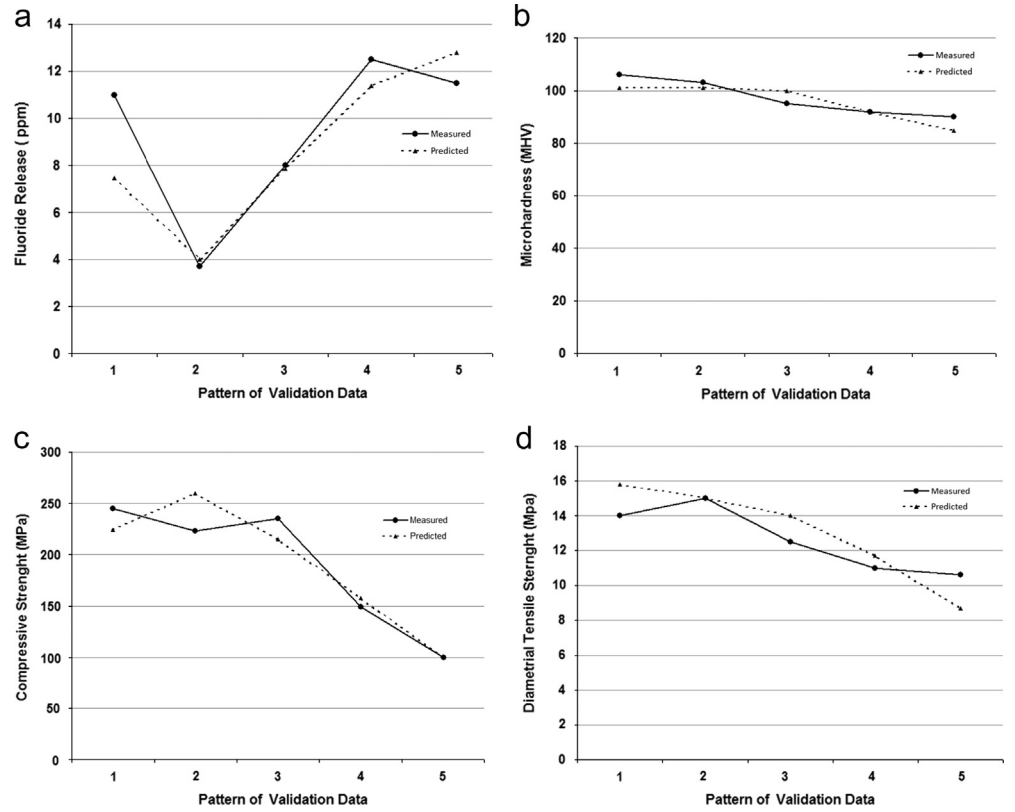

Fig. 13 – The comparison of the measured and the predicted data for the test stage of fluoride release (a), microhardness (b), compressive strength (c) and diametral tensile strength (d) of HA/YSZ–GIC after 7 days immersion.

4. Conclusion

In this research a ternary nanocomposite, HA/YSZ, was successfully synthesized by using the sol–gel method. According to STA analysis, 750 °C was chosen as the calcination temperature of the composite. Structural analysis demonstrated the stabilization of HA and the formation of t-ZrO_2 in the synthetic condition. Crystallization of t-ZrO_2 occurred in the presence of 3 mol% of Y_2O_3.

The prepared nanocomposite was examined to modify the expected features of GIC. The results illustrated that a combination of 20 wt% HA besides 80 wt% of YSZ acted as a remarkable GIC reinforcement agent. It was also found that fluoride release profile of GIC was highly improved in the presence of 5 wt% of HA/YSZ. Mechanical properties of HA/YSZ–loaded GIC were improved by increasing the soaking time due to the development of aluminum salt bridges.

The feed forward neural network was employed to model the performance of GIC in the presence of the HA/YSZ nanocomposite. The predicted values for mechanical properties and fluoride release of GIC were in a close accordance with the result obtained from the experiment.

Acknowledgments

The authors would like to thank the Khorasan Science and Technology Park, for kindly providing the equipment and materials.

REFERENCES

Balamurugan, A., Balossier, G., Kannan, S., Michel, J., Rajeswari, S., 2007. Materials Science and Engineering C 27, 162.
Cales, B., Stefani, Y., Lilley, E., 1994. Journal of Biomedical Materials Research 28, 619.
Chandradass, J., Han, K.S., Bae, D.S., 2008. Journal of Materials Processing Technology 206, 315.
Chiu, C.Y., Hsu, H.C., Tuan, W.H., 2007. Ceramics International 33, 715.
Dental Standards Committee, BS 6039:1981, 1981. British Standard Specification for Dental Glass Ionomer Cements. British Standard Institution.
Dhondt, C.L., Maeyer, E.A.P., Verbeeck, R.M.H., 2001. Journal of Dental Research 80, 1402.
Feng, W., Sena, L.M., Penga, L.Y., Xin, Q.B.D.Y., 2005. Materials Letters 59, 916.
Goenka, S., Balub, R., Kumar, T.S.S., 2012. Journal of the Mechanical Behavior of Biomedical Materials 7, 69.
Gu, Y.W., Yap, A.U.J., Cheang, P., Khor, K.A., 2005a. Biomaterials 26, 713.
Gu, Y.W., Yap, A.U.J., Cheang, P, Khor, KA, 2005b. Journal of Non-Crystalline Solids 51, 508.
Guo, H., Khor, K.A., Boey, Y.C., Miao, X., 2003. Biomaterials 24, 667.
Heffernan, M.J., Aquilino, S.A., Diaz-Arnold, A.M., Haselton, D.R., Stanford, C.M., Vargas, M.A., 2002. Journal of Prosthetic Dentistry 88, 4.
Hwang, R.C., Chen, Y.J., Huang, H.C., 2010. Expert Systems with Applications 37, 3136.
Lee, T.M., Tsai, R.S., Chang, E., Yang, C.Y., Yang, M.R., 2002. Journal of Materials Science—Materials in Medicine 13, 281.
Lucas, M.E., Arita, K., Nishino, M., 2003. Biomaterials 24, 3787.
Monte, F.D., Larsen, W., Mackenzie, J.D., 2000. Journal of American Ceramic Society 83, 628.
Moshaverinia, A., Ansari, S., Movasaghi, Z., Billington, R.W., Darr, J.A., Rehman, I.U., 2008. Dental Materials 2 (4), 1381.
Noort, V.R., 1994. Introduction to dental materials. Times Mirror International, Mosby Wolfe, London, UK.
Ozerdem, M.S., Kolukisa, S., 2009. Materials & Design 30, 764.
Piconi, C., Maccauro, G., 1999. Biomaterials 20, 1.
Salehi, S., Fathi, M.H., 2010. Ceramics International 36, 1659.
Samanipour, F., Bayati, M.R., Zargar, H.R., Golestani-Fard, F., Troczynskic, T., Taheri, M., 2011. Journal of Alloys and Compounds 509, 9351.
Sanosh, K.P., Chu, M.C., Balakrishnan, A., Lee, Y.J., Kim, T.N., Cho, S.J., 2009. Current Applied Physics 9, 1459.
Silva, V.V., Lameiras, F.S., 2000. Materials Characterization 45, 51.
Sung, Y.M., Shin, Y.K., Ryu, J.J., 2007. Nanotechnology 18, 065602.
Uo, M., Sjoren, G., Sundh, A., Watari, F., Bergman, M., Lerner, U., 2003. Dental Materials 19, 487.
Wilson, A.D., Kent, B.E., 1971. Journal of Applied Chemistry & Biotechnology 21, 313.
Zhan, Z., Zeng, H.C., 1999. Journal of Non-Crystalline Solids 243, 26.